

# Dynamics of allosteric transitions in GroEL

Changbong Hyeon<sup>†</sup>, George H. Lorimer<sup>†§¶</sup>, and D. Thirumalai<sup>†§¶</sup>

<sup>†</sup>Biophysics Program Institute for Physical Science and Technology and <sup>§</sup>Department of Chemistry and Biochemistry, University of Maryland, College Park, MD 20742

Contributed by George H. Lorimer, October 3, 2006 (sent for review September 2, 2006)

The chaperonin GroEL-GroES, a machine that helps proteins to fold, cycles through a number of allosteric states, the *T* state, with high affinity for substrate proteins, the ATP-bound *R* state, and the *R'* (GroEL-ADP-GroES) complex. Here, we use a self-organized polymer model for the GroEL allosteric states and a general structure-based technique to simulate the dynamics of allosteric transitions in two subunits of GroEL and the heptamer. The *T* → *R* transition, in which the apical domains undergo counterclockwise motion, is mediated by a multiple salt-bridge switch mechanism, in which a series of salt-bridges break and form. The initial event in the *R* → *R'* transition, during which GroEL rotates clockwise, involves a spectacular outside-in movement of helices K and L that results in K80-D359 salt-bridge formation. In both the transitions there is considerable heterogeneity in the transition pathways. The transition state ensembles (TSEs) connecting the *T*, *R*, and *R'* states are broad with the TSE for the *T* → *R* transition being more plastic than the *R* → *R'* TSE.

allostery | self-organized polymer model

The hallmark of allostery in biomolecules is the conformational changes at distances far from the sites at which ligands bind (1–3). The potential link between large scale allosteric transitions and function is most vividly illustrated in biological nanomachines (4, 5). Sequence (6–8) or structure-based (9, 10) methods have been proposed to predict the allosteric wiring diagram. However, to fully understand the role of allostery it is important to dynamically monitor the structural changes that occur in the transition from one state to another (11–15). Here, we propose a method for determining allosteric mechanisms in biological systems with applications to dynamics of such processes in the chaperonin GroEL, an ATP-fueled nanomachine, which facilitates folding of proteins [substrate proteins (SPs)] that are otherwise destined to aggregate (16, 17).

GroEL has two heptameric rings, stacked back-to-back. SPs are captured by GroEL in the *T* state (Fig. 1) while ATP-binding triggers a transition to the *R* state. Binding of the co-chaperonin GroES requires dramatic movements in the A domains which double the volume of the central cavity. Comparison of the structures of the *T*, *R*, and the *R'* [GroEL-(ADP)<sub>7</sub>-GroES] indicates that the equatorial (E) domain, which serves as an anchor (16), undergoes comparatively fewer structural changes. Although structural and mutational studies (18–20) have identified many residues that affect GroEL function, only few studies have explored the dynamics of allosteric transitions between the various states (21–23).

Here, we use the self-organized polymer model of GroEL and a novel technique (see *Methods*) to monitor the order of events in the *T* → *R*, *R* → *R'*, and *T* → *R'* transitions. By simulating the dynamics of ligand-induced conformational changes in the heptamer and also in two subunits, we have obtained an unprecedented view of the key interactions that drive the various allosteric transitions. The transitions between the states are induced (see *Methods*) under the assumption that the rate of conformational changes is slower than the rate at which ligand-binding induced strain propagates. The simplicity of the self-organized polymer model allowed us to generate multiple trajectories to resolve the key events in the allosteric transitions. We make a number of predictions including the identification of a multiple salt-bridge switch mechanism in the

*T* → *R* transition, and the occurrence of dramatic movement of helices K and L in the *R* → *R'* transition. The structures of the transition state ensembles (TSEs) that connect the end points show considerable variability mostly localized in the A domain.

## Results and Discussion

### Heptamer Dynamics Show That the A Domains Rotate Counterclockwise in the *T* → *R* Transition and Clockwise in the *R* → *R'* Transition.

To probe the global motions in the various stages of GroEL allostery we simulated the entire heptamer (see *Methods*). The dynamics of the *T* → *R* transition, monitored using the time-dependent changes in the angles  $\alpha$ ,  $\beta$ , and  $\gamma$  (see the legend of Fig. 2 for definitions), that measure the relative orientations of the subunits, show (Fig. 2*A*) that the A domains twist in a counterclockwise manner in agreement with experiment (24). The net changes in the angles in the *R* → *R'* transition, which occurs in a clockwise direction (Fig. 2*B*), is greater than in the *T* → *R* transition. As a result the global *T* → *R'* transition results in a net  $\approx 110^\circ$  rotation of the A domains. Surprisingly, there are large variations in the range of angles explored by the individual subunits during the *T* → *R* → *R'* transitions. There are many more intersubunit contacts in the E domain than in the A domain, thus permitting each A domain to move independently of one another. Fig. 2 shows that the dynamics of each subunit is distinct despite the inference, from the end states alone, that the overall motion occurs without significant change in the root mean square deviation (RMSD) of the individual domains. The time-dependent changes in the angles  $\alpha$ ,  $\beta$ , and  $\gamma$  from one subunit to another are indicative of an inherent dynamic asymmetry in the individual subunits that has been noted in static structures (25, 26). As in the *T* → *R* transition, there is considerable dispersion in the time-dependent changes in  $\alpha$ ,  $\beta$ , and  $\gamma$  of the individual subunits (Fig. 2*B*) during the *R* → *R'* transition.

The clockwise rotation of apical domain alters the nature of lining of the SP binding sites (domain color-coded in magenta in Fig. 1). The dynamic changes in the  $\gamma$  angle (Fig. 2) associated with the hinge motion of the I domain that is perpendicular to the A domain lead to an expansion of the overall volume of the heptamer ring. More significant conformational changes, that lead to doubling of the volume of the cavity, take place in the *R* → *R'* transition. The apical domain is erected, so that the SP binding sites are oriented upwards providing binding interfaces for GroES. Some residues, notably 357–361, which are completely exposed on the exterior surface in the *T* state move to the interior surface during the *T* → *R* → *R'* transitions.

### Global *T* → *R* and *R* → *R'* Transitions Follow Two-State Kinetics.

Time-dependent changes in RMSD with respect to a reference state (*T*, *R*, or *R'*), from which a specific allosteric transition commences

Author contributions: C.H., G.H.L., and D.T. designed research; C.H. and D.T. performed research; C.H., G.H.L., and D.T. analyzed data; and C.H., G.H.L., and D.T. wrote the paper.

The authors declare no conflict of interest.

Abbreviations: RMSD, root mean square deviation; SP, substrate protein; TS, transition state; TSE, TS ensemble.

<sup>¶</sup>To whom correspondence may be addressed. E-mail: glorimer@umd.edu or thirum@glue.umd.edu.

© 2006 by The National Academy of Sciences of the USA

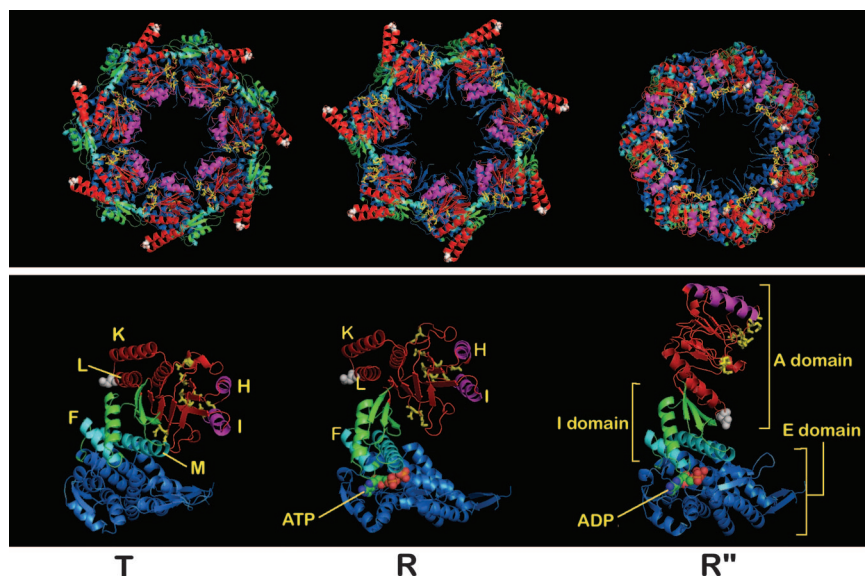


**Fig. 1.** GroEL structure. From left to right, *T*, *R*, and *R'* structures of GroEL structures are shown. The top view is given in *Upper* (for a side view, see Fig. 7, which is published as supporting information on the PNAS web site), and *Lower* displays the side view of a single subunit. The white ball represents D359. The helices that most directly influence the allosteric transitions are labeled.

(Fig. 3), differ from molecule to molecule (Fig. 3*A*). Examination of the RMSD for a particular trajectory in the transition region (Fig. 3*A Inset*) shows that the molecule undergoes multiple passages through the transition state (TS). GroEL spends a substantial fraction of time (measured with respect to the first passage time) in the TS region during the *T* → *R* transition. The ensemble average of the time-dependence of RMSD for both the *T* → *R* and *R* → *R'* transitions follow single exponential kinetics. Despite a broad transition region, the allosteric transitions can be approximately described by a two-state model.

***T* → *R* Transition Is Triggered by Downward Tilt of Helices F and M in the I-Domain Followed by a Multiple Salt-Bridge Switching Mechanism.** Several residues in helices F (141–151) and M (386–409) in the I domain interact with the nucleotide-binding sites in the E domain thus creating a tight nucleotide binding pocket. The favorable interactions are enabled by the F, M helices tilting by ≈15° that results in the closing of the nucleotide-binding sites. A number of residues around the nucleotide binding pocket are highly conserved (27, 28). Because the *T* → *R* transition involves the formation and breakage of intra- and intersubunit contacts, we simulated two

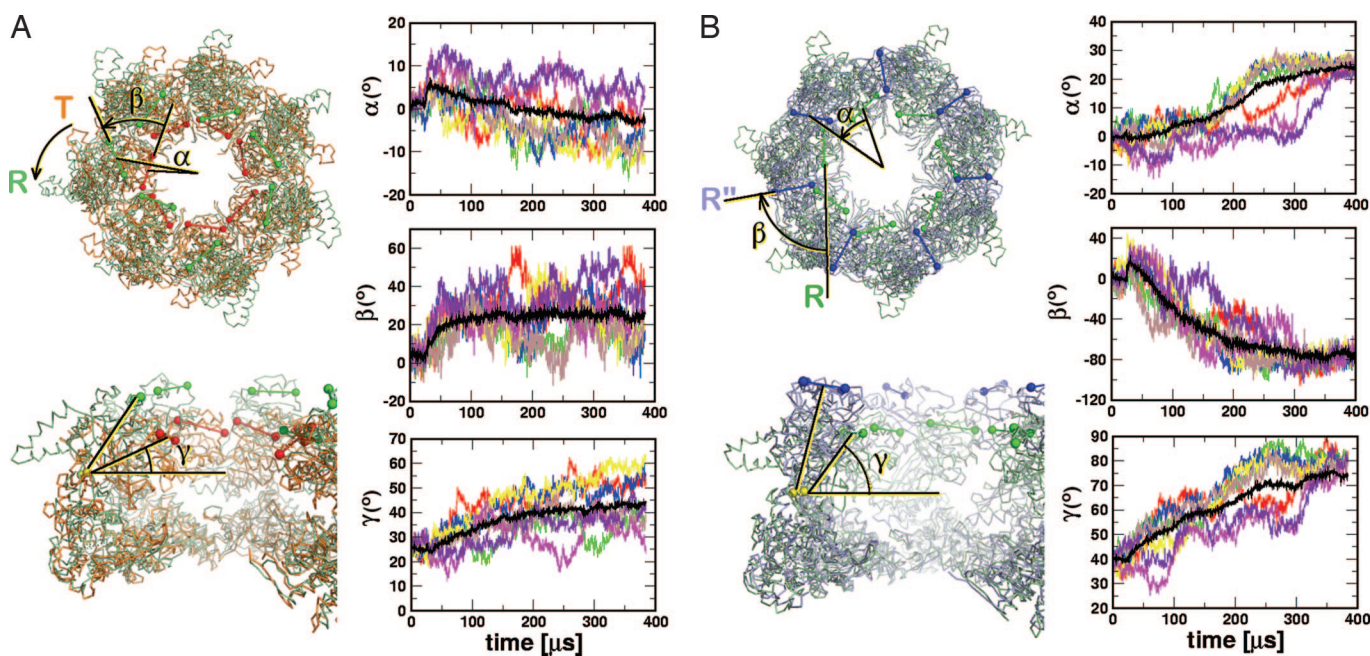


**Fig. 2.** GroEL dynamics monitored using various angles. (A) *T* → *R* transition dynamics for the heptamer monitored using angles  $\alpha$ ,  $\beta$ , and  $\gamma$ . An angle  $\theta$  ( $= \alpha, \beta$ ) is defined by  $\cos\theta(t) = \vec{u}_\theta(0) \cdot \vec{u}_\theta(t) / |\vec{u}_\theta(0)| |\vec{u}_\theta(t)|$ . For  $\alpha$ , we obtain  $\vec{u}_\alpha(t)$  by projecting the vector ( $\vec{r}_{236(i)}(t) = \vec{R}_{236(i)}(t) - \vec{R}_{CM}$ ) between the center of mass ( $\vec{R}_{CM}$ ) and residue 236 on *i*th subunit [ $\vec{R}_{236(i)}(t)$ ] onto the plane perpendicular to the principal axis ( $\hat{e}_p$ ) of the heptamer, i.e.,  $\vec{u}_\alpha(t) = \vec{r}_{236(i)}(t) - (\vec{r}_{236(i)}(t) \cdot \hat{e}_p) \hat{e}_p$ . The angle between H helices (residue 231–242) of *i*th subunit at times  $t = 0$  and  $t$  using the vector,  $\vec{R}_{231(i)}(t) - \vec{R}_{242(i)}(t)$  is  $\beta$ . The sign of the angles ( $\alpha$  and  $\beta$ ) is determined using  $\text{sgn}[(\vec{u}(0) \times \vec{u}(t)) \cdot \hat{e}_p]$ , which is (+) for counterclockwise and (−) for clockwise rotation.  $\gamma$  measures the perpendicular motion of apical domain with respect to the hinge (residue 377). We defined  $\vec{u}_\gamma(t) = \vec{R}_{236(i)}(t) - \vec{R}_{377(i)}(t)$  at each subunit *i*, and  $\gamma(t) = 90^\circ - \cos^{-1}(\vec{u}_\gamma \cdot \hat{e}_p)$ . In *A Right* we plot the time dependence of  $\alpha$ ,  $\beta$ , and  $\gamma$  for each subunit in different color. The black line represents the average of 21 ( $= 3 \times 7$ ) values of each angle calculated from three trajectories of 7 subunits. (B) Same as in *A* except for the *R* → *R'* transition.





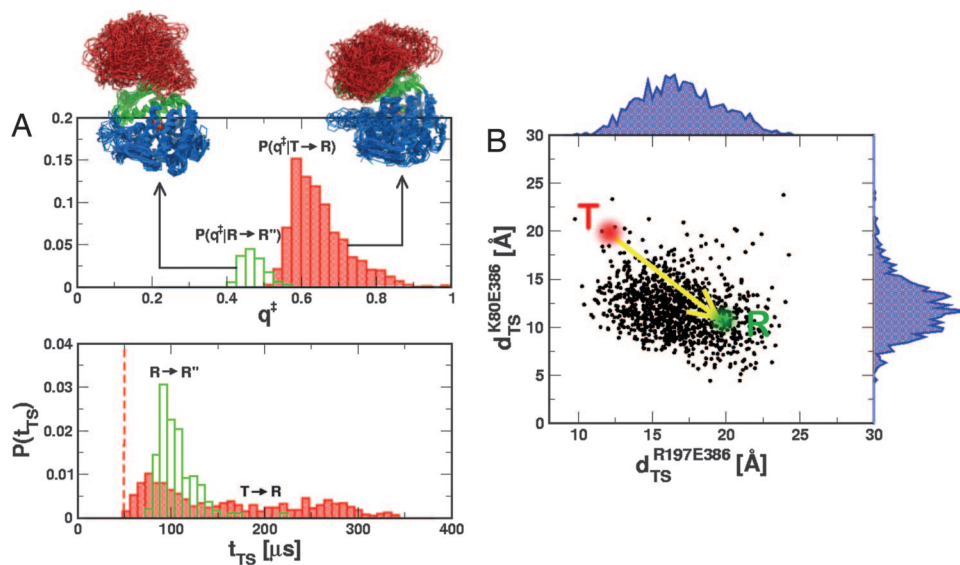


**Fig. 6.** TSEs. (A) TSEs are represented in terms of distributions  $P(q^\ddagger)$ , where  $q^\ddagger \equiv \Delta^\ddagger - \min(\text{RMSD}/X)/\max(\text{RMSD}/X) - \min(\text{RMSD}/X)$ . Histogram in red gives  $P(q^\ddagger)$  for  $T \rightarrow R$  (red) and the data in green are for the  $R \rightarrow R''$  transitions. For  $T \rightarrow R$ ,  $X = R$ ,  $\min(\text{RMSD}/X) = 1.5 \text{ \AA}$ , and  $\max(\text{RMSD}/X) = 8.0 \text{ \AA}$ . For  $R \rightarrow R''$ ,  $X = R''$ ,  $\min(\text{RMSD}/X) = 1.5 \text{ \AA}$ , and  $\max(\text{RMSD}/X) = 14.0 \text{ \AA}$ . To satisfy conservation of the number of molecules the distributions are normalized by using  $\int dq^\ddagger [P(q^\ddagger)T \rightarrow R] + P(q^\ddagger)R \rightarrow R'' = 1$ . Twenty overlapped TSE structures for the two transitions are displayed. (Lower) Distributions of  $t_{\text{TS}}$  that satisfy  $\delta^\ddagger < 0.2 \text{ \AA}$  plotted for the  $T \rightarrow R$  TSE and the  $R \rightarrow R''$  transitions. (B) For the  $T \rightarrow R$  TSE we show the salt-bridge distances ( $d_{\text{TS}}^{R197-E386}$ ,  $d_{\text{TS}}^{K80-E386}$ ) with black dots. The red and the green dots are the equilibrium distances ( $\langle d_{\text{TS}}^{R197-E386} \rangle$ ,  $\langle d_{\text{TS}}^{K80-E386} \rangle$ ) in the  $T$  and the  $R$  states, respectively. The distance distributions for the TSE are shown in blue.

outside-in motion facilitates the K80-D359 salt-bridge formation which in turn orients the position of the wing. The orientation of the apical domain's wing inside the cylinder exerts a substantial strain (data not shown) on the GroEL structure. To relieve the strain, the apical domain is forced to undergo a dramatic  $90^\circ$  clockwise rotation and  $40^\circ$  upward movement with respect to the  $R$  state. As a result, the SP binding sites (H, I helices) are oriented in the upward direction. Before the strain-induced alterations are possible the distance between K80 and D359 decreases drastically from that in  $R$  state (Fig. 5 *Center Middle*). The clockwise motion of the apical domain occurs only after the formation of salt-bridge between K80 and D359. On the time scale during which K80-D359 salt-bridge forms, the rupture kinetics of several interapical domain salt-bridges involving residues K245, E257, R268, K321, and R322 follow complex kinetics (Fig. 5). Formation of contact between I305 and A260 (a binding site for SPs), and intersubunit residue pair located at the interface of two adjacent apical domains in the  $R''$  state, occurs extremely slowly compared with others. The nonmonotonic and lag-phase kinetics observed in the rupture and formation of a number of contacts suggests that intermediate states must exist in the pathways connecting the  $R$  and  $R''$  states.

The clockwise rotation of apical domain, that is triggered by a network of salt-bridges as well as interactions between hydrophobic residues at the interface of subunits, orients it in the upward direction so as to permit the binding of the mobile loop of GroES. Hydrophobic interactions between SP binding sites and GroES drive the  $R \rightarrow R''$  transition. The hydrophilic residues, that are hidden on the side of apical domain in the  $T$  or the  $R$  state, are now exposed to form an interior surface of the GroEL (see the residue colored in yellow on the A domain in Fig. 1). The E409-R501 salt-bridge formed between I and A domains close to the  $\gamma - P_i$  binding site is maintained throughout the allosteric transitions including in the transition state (31).

**TSEs Are Broad.** The structures of the TSEs connecting the  $T$ ,  $R$ , and  $R''$  states are obtained using RMSD as a surrogate reaction coordinate. We assume that the TS location is reached when  $\delta^\ddagger = |(\text{RMSD}/T)(t_{\text{TS}}) - (\text{RMSD}/R)(t_{\text{TS}})| < r_c$ , where  $r_c = 0.2 \text{ \AA}$  and  $t_{\text{TS}}$  is the time at which  $\delta^\ddagger < r_c$ . Letting the value of RMSD at the TS be  $\Delta^\ddagger = 1/2 \times |(\text{RMSD}/T)(t_{\text{TS}}) + (\text{RMSD}/R)(t_{\text{TS}})|$ , the distributions  $P(\Delta^\ddagger)$  for  $T \rightarrow R$  and  $R \rightarrow R''$  transitions are broad (see Fig. 9, which is published as sup-

porting information on the PNAS web site). If  $\Delta^\ddagger$  is normalized by the RMSD between the two end point structures to produce a Tanford  $\beta$ -like parameter  $q^\ddagger$  (see legend of Fig. 6 for definition), we find that the width of the TSE for the  $R \rightarrow R''$  is less than the  $T \rightarrow R$  transition (Fig. 6A). The mean values of  $q^\ddagger$  for the two transitions show that the most probable TS is located close to the  $R$  states in both  $T \rightarrow R$  and  $R \rightarrow R''$  transitions.

Disorder in the TSE structures (Fig. 6) is largely localized in the A domain which shows that the substructures in this domain partially unfold as the barrier crossings occur. By comparison the E domain remains more or less structurally intact even at the transition state which suggests that the relative immobility of this domain is crucial to the function of this biological nanomachine (16). The dispersions in the TSE are also reflected in the heterogeneity of the distances between various salt-bridges in the transition states. The values of the contact distances, in the  $T \rightarrow R$  transition among the residues involved in the salt-bridge switching between K80, R197, and E386 at the TS has a very broad distribution (Fig. 6B) which also shows that the R197-E386 is at least partially disrupted in the TS and the K80-E386 is partially formed (32).

## Conclusions

We have developed a structure-based method to probe the allosteric transitions in biological molecules. Applications to allosteric transitions in GroEL have produced a number of new predictions that can be experimentally tested. The transitions occur by a coordinated switch between a network of multiple salt-bridges. The most dramatic outside-in movement, the rearrangement of helices K and L of the A domain, occurs largely in the  $R \rightarrow R''$  transition and results in the intersubunit K80-D359 salt-bridge formation. In both the transitions most of the conformational changes occur in the A domain with the E domain serving as a largely structurally unaltered static base that is needed for force transmission (16).

## Methods

**Energy Function.** Using the available structures in the Protein Data Bank [PDB entries 1OEL ( $T$  state) (33), 2C7E ( $R$  state) (24), and 1AON ( $R''$  state) (34)], the *state-dependent* self-organized polymer Hamiltonian (35, 36) of the states ( $X = T, R, R''$ ) of GroEL is

$H(\{\tilde{r}_i\}|X)$

$$\begin{aligned}
 &= H_{\text{FENE}} + H_{\text{nb}}^{\text{(att)}} + H_{\text{nb}}^{\text{(rep)}} + H_{\text{ATP}}^{\text{(att)}} + H_{\text{ATP}}^{\text{(rep)}} + H_{\text{sb}} \\
 &= - \sum_{i=1}^{N-1} \frac{k}{2} R_0^2 \log \left( 1 - \frac{(r_{i,i+1} - r_{i,i+1}^o(X))^2}{R_0^2} \right) \\
 &+ \sum_{i=1}^{N-3} \sum_{j=i+3}^N \epsilon_h \left[ \left( \frac{r_{ij}^o(X)}{r_{ij}} \right)^{12} - 2 \left( \frac{r_{ij}^o(X)}{r_{ij}} \right)^6 \right] \Delta_{ij}(X) \\
 &+ \left[ \sum_{i=1}^{N-2} \epsilon_l \left( \frac{\sigma}{r_{i,i+2}} \right)^6 + \sum_{i=1}^{N-3} \sum_{j=i+3}^N \epsilon_l \left( \frac{\sigma}{r_{ij}} \right)^6 (1 - \Delta_{ij}(X)) \right] \quad [1] \\
 &+ \sum_{i=1}^N \sum_{j \in \text{ATP or ADP}} \epsilon_h^{\text{ATP}} \left[ \left( \frac{a_{ij}^o(X)}{r_{ij}} \right)^{12} - 2 \left( \frac{a_{ij}^o(X)}{r_{ij}} \right)^6 \right] \Delta_{ij}(X) \\
 &+ \sum_{i=1}^N \sum_{j \in \text{ATP or ADP}} \epsilon_l^{\text{ATP}} \left( \frac{\sigma}{r_{ij}} \right)^6 (1 - \Delta_{ij}(X)) \\
 &+ \sum_{i^*, j^* \in \{\text{salt bridge}\}} \frac{q_1 q_2}{4\pi\epsilon r_{ij}} e^{-\kappa r_{ij}}.
 \end{aligned}$$

The first term, which accounts for chain connectivity, is given by the finite extensible nonlinear elastic (FENE) potential (37), with parameters  $k = 20 \text{ kcal}/(\text{mol}\cdot\text{\AA}^2)$ ,  $R_0 = 2 \text{ \AA}$ , where  $r_{i,i+1}$  is the distance between neighboring interaction centers  $i$  and  $i + 1$ , and  $r_{i,i+1}^o(X)$  is the distance in state  $X$ . The Lennard–Jones potential (second term) accounts for interactions that stabilize a particular allosteric state. Native contact exists if the distance between  $i$  and  $j$  is  $< R_C = 8 \text{ \AA}$  in state  $X$  for  $|i - j| > 2$ . If  $i$  and  $j$  sites are in contact in the native state,  $\Delta_{ij} = 1$ , otherwise  $\Delta_{ij} = 0$ . To ensure the noncrossing of the chain, we used a 6th power potential in the third and the fifth terms and set  $\sigma = 3.8 \text{ \AA}$ , which is the  $C^\alpha$ – $C^\alpha$  distance. We used  $\epsilon_h = 2 \text{ kcal/mol}$  if the residues are in contact and  $\epsilon_l = 1 \text{ kcal/mol}$  for nonnative pairs.

The fourth and the fifth terms in Eq. 1 are for interaction of residues with ATP ( $R$  state) or ADP ( $R'$  state). The atomic coordinates of ATP (ADP) are taken from the  $R$  ( $R'$ ) structure without coarse-graining. The functional form for residue-ATP (or ADP) interaction is the same as for residue-residue interactions with  $\epsilon_h^{\text{ATP}} = 0.2 \text{ kcal/mol}$ ,  $\epsilon_l^{\text{ATP}} = 0.1 \text{ kcal/mol}$ . We used a small

value of  $\epsilon_h^{\text{ATP}}$  (or  $\epsilon_l^{\text{ATP}}$ ) because the coordinates of all of the heavy atoms of ATP and ADP are explicitly used as interaction sites. The distance between the  $i$ th residue and the  $j$ th atom in ATP (or ADP) is  $a_{ij}$ . We used the screened electrostatic potential where  $\kappa^{-1} = 2.4 \text{ \AA}$ ,  $\epsilon = 10\epsilon_0$ , and  $q_1 q_2 = -e^2$  to account for the favorable salt-bridge interactions that are state-independent (Eq. 1).

**Inducing Allosteric Transitions.** The  $T \rightarrow R$  allosteric transition of GroEL is simulated by integrating the equations of motion with the force arising from  $H(\{\tilde{r}_i\}|R)$ . The ensemble of initial structures were generated using the T-state  $H(\{\tilde{r}_i\}|T)$ . The Brownian dynamics algorithm (38, 39) determines the configuration of GroEL at time  $t$  as follows:

$$\begin{aligned}
 &(i) \zeta \tilde{r}_i(t + h) = \zeta \tilde{r}_i(t) + h(\tilde{F}_i(t|T) + \tilde{\Gamma}_i(t)) \quad (0 \leq t < t^*) \\
 &(ii) \zeta \tilde{r}_i(t + h^*) = \zeta \tilde{r}_i(t) + h^*(\tilde{F}_i(t|T \rightarrow R) + \tilde{\Gamma}_i(t)) \\
 &\quad (t^* \leq t < t^* + N_i h^*) \quad [2] \\
 &(iii) \zeta \tilde{r}_i(t + h) = \zeta \tilde{r}_i(t) + h(\tilde{F}_i(t|R) + \tilde{\Gamma}_i(t)) \quad (t \leq t^* + N_i h^*),
 \end{aligned}$$

where  $\tilde{F}_i(t|X) = -\nabla_{\tilde{r}_i} H(\{\tilde{r}_i\}|X)$  ( $X = T, R$ , or  $T \rightarrow R$ ), and  $\tilde{\Gamma}_i(t)$  is a random force on  $i$ th residue that has a white noise spectrum.

The algorithm in Eq. 2 is implemented in three steps: (i) during the time interval  $0 \leq t < t^*$  an ensemble of T-state conformations is generated; (ii) the energy function is switched from  $H(\{\tilde{r}_i\}|T)$  to  $H(\{\tilde{r}_i\}|R)$  symbolized by  $H(\{\tilde{r}_i\}|T \rightarrow R)$  in the duration  $t^* \leq t < t^* + N_i h^*$  (if  $N_i = 0$  our method is similar to one in ref. 14); and (iii) a dynamic trajectory under  $H(\{\tilde{r}_i\}|R)$  is generated for  $t > t^*$ . The assumption in our method is that the rate of conformational change in biomolecules is smaller than the rate at which a locally applied strain (because of ligand binding) propagates. As a result, the Hamiltonian switch should not be instantaneous ( $N_i \neq 0$ ). Using a nonzero value of  $N_i$  (second step in Eq. 2) not only ensures that there is a lag time between ligand binding and the associated response but also eliminates computational instabilities in the distances between certain residues that change dramatically during the transition. The “loading” rate can be altered by varying  $N_i$  and hence even nonequilibrium ligand-induced transitions can be simulated. Additional details of the simulations are given in *Supporting Text*, which is published as supporting information on the PNAS web site.

This work was supported in part by National Institutes of Health Grant 1R01 GM067851-01.

- Perutz MF (1989) *Q Rev Biophys* 22:139–237.
- Changeux JP, Edelstein SJ (2005) *Science* 308:1424–1428.
- Horowitz A, Willison KR (2005) *Curr Opin Struct Biol* 15:646–651.
- Doublet S, Sawaya MR, Ellenberger T (1999) *Structure (London)* 7:R31–R35.
- Kern D, Zuiderweg ER (2003) *Curr Opin Struct Biol* 13:748–757.
- Lockless SW, Ranganathan R (1999) *Science* 286:295–299.
- Kass I, Horowitz A (2002) *Protein Struct Funct Genetics* 48:611–617.
- Dima RI, Thirumalai D (2006) *Protein Sci* 15:258–268.
- Zheng W, Brooks BR, Doniach S, Thirumalai D (2005) *Structure (London)* 13:565–577.
- Zheng W, Brooks BR, Thirumalai D (2006) *Proc Natl Acad Sci USA* 103:7664–7669.
- Bahar I, Rader AJ (2005) *Curr Opin Struct Biol* 15:586–592.
- Miyashit O, Onuchic JN, Wolynes PG (2003) *Proc Natl Acad Sci USA* 100:12570–12575.
- Best RB, Chen YG, Hummer G (2005) *Structure (London)* 13:1755–1763.
- Koga N, Takada S (2006) *Proc Natl Acad Sci USA* 103:5367–5372.
- Okazaki K, Koga N, Takada S, Onuchic JN, Wolynes PG (2006) *Proc Natl Acad Sci USA* 103:11844–11849.
- Thirumalai D, Lorimer GH (2001) *Annu Rev Biophys Biomol Struct* 30:245–269.
- Horwich AL, Farr GW, Fenton WA (2006) *Chem Rev* 106:1917–1930.
- Horowitz A, Bochkareva ES, Yifrach O, Girshovich AS (1994) *J Mol Biol* 238:133–138.
- Horowitz A, Fridmann Y, Kafri G, Yifrach O (2001) *J Struct Biol* 135:104–114.
- Yifrach O, Horowitz A (1995) *Biochemistry* 34:5303–5308.
- Ma J, Karplus M (1998) *Proc Natl Acad Sci USA* 95:8502–8507.
- Ma J, Sigler PB, Xu Z, Karplus M (2000) *J Mol Biol* 302:303–313.
- Chennubhotla C, Bahar I (2006) *Mol Syst Biol* 2:msb4100075.
- Ranson NA, Farr GW, Roseman AM, Gowen B, Fenton WA, Horwich AL, Saibil HR (2001) *Cell* 107:869–879.
- Danzinger O, Rivenzon-Segal D, Wolf SG, Horowitz A (2003) *Proc Natl Acad Sci USA* 100:13797–13802.
- Shimamura T, Takeshita AK, Yokoyama K, Masui R, Murai N, Yoshida M, Taguchi H, Iwata S (2004) *Structure (London)* 12:1471–1480.
- Brocchieri L, Karlin S (2000) *Protein Sci* 9:476–486.
- Stan G, Thirumalai D, Lorimer GH, Brooks BR (2003) *Biophys Chem* 100:453–467.
- Stan G, Brooks BR, Thirumalai D (2005) *J Mol Biol* 350:817–829.
- Danzinger O, Shimon L, Horowitz A (2006) *Protein Sci* 15:1270–1276.
- Aharoni A, Horowitz A (1997) *Proc Natl Acad Sci USA* 94:1698–1702.
- Horowitz A, Amir A, Danzinger O, Kafri G (2002) *Proc Natl Acad Sci USA* 99:14095–14097.
- Braig K, Adams PD, Brunger AT (1995) *Nat Struct Biol* 2:1083.
- Xu Z, Horwich AL, Sigler PB (1997) *Nature* 388:741.
- Hyeon C, Dima RI, Thirumalai D (2006) *Structure (London)* 14:1633–1645.
- Hyeon C, Thirumalai D (2006) *Biophys J*, in press.
- Kremer K, Grest GS (1990) *J Chem Phys* 92:5057–5086.
- Ermak DL, McCammon JA (1978) *J Chem Phys* 69:1352–1369.
- Veitshans T, Klimov DK, Thirumalai D (1996) *Folding Des* 2:1–22.